Cancer Letters 458 (2019) 76–85

Contents lists available at ScienceDirect

Cancer Letters

journal homepage: www.elsevier.com/locate/canlet

Original Articles

Novel ROR1 inhibitor ARI-1 suppresses the development of non-small cell lung cancer

Xuesha Liu[a,1], Wenchen Pu[a,1], Huaiyu He[a], Xin Fan[a,b], Yuanyuan Zheng[a], Jian-Kang Zhou[a], Rui Ma[a], Juan He[a], Yuzhu Zheng[a], Ke Wu[a], Yun Zhao[b], Sheng-Yong Yang[a], Chun Wang[c], Yu-Quan Wei[a], Xia-Wei Wei[a,**], Yong Peng[a,*]

[a] State Key Laboratory of Biotherapy and Cancer Center, National Clinical Research Center for Geriatrics, West China Hospital, Sichuan University, Chengdu 610041, China
[b] College of Life Science, Sichuan University, Chengdu 610065, China
[c] Chengdu Institute of Biology, Chinese Academy of Sciences, Chengdu 610041, China

ARTICLE INFO

Keywords:
NSCLC
ROR1
EGFR-TKIs
Inhibitor
PI3K/AKT pathway

ABSTRACT

Limited drug response and severe drug resistance confer the high mortality of non-small-cell lung cancer (NSCLC), a leading cause of cancer death worldwide. There is an urgent need for novel treatment against NSCLC. Receptor tyrosine kinase-like orphan receptor 1 (ROR1) is aberrantly overexpressed and participats in NSCLC development and EGFR-TKIs-induced drug resistance. Increasing evidences indicate that oncogenic ROR1 is a potential target for NSCLC therapy. However, nearly no ROR1 inhibitor was reported until now. Here, combining the computer-aided drug design and cell-based activity screening, we discover (*R*)-5,7-bis(methoxymethoxy)-2-(4-methoxyphenyl)chroman-4-one (ARI-1) as a novel ROR1 inhibitor. Biological evaluation demonstrates that ARI-1 specifically targets the extracellular frizzled domain of ROR1 and potently suppresses NSCLC cell proliferation and migration by regulating PI3K/AKT/mTOR signaling in a ROR1-dependent manner. Moreover, ARI-1 significantly inhibits tumor growth *in vivo* without obvious toxicity. Intriguingly, ARI-1 is effective to EGFR-TKIs-resistant NSCLC cells with high ROR1 expression. Therefore, our work suggests that the ROR1 inhibitor ARI-1 is a novel drug candidate for NSCLC treatment, especially for EGFR-TKIs-resisted NSCLC with high ROR1 expression.

1. Introduction

Lung cancer is the leading cause of cancer-associated human death worldwide with a 5-year survival rate of only 18% [1]. A histological subgroup collectively known as non-small cell lung cancer (NSCLC), approximately 85% of all lung cancer cases, is usually diagnosed at an advanced stage and had a poor prognosis [2,3]. Epidermal growth factor receptor-tyrosine kinase inhibitors (EGFR-TKIs), including gefitinib, afatinib and erlotinib, are FDA-approved first-line therapy for advanced NSCLC [4]. However, limited drug response and severe drug resistance as a result of EGFR-TKIs-induced secondary EGFR T790 M or C797S mutations or alternative oncogenic gene variations [5–7] summon new targets for NSCLC treatment.

Receptor tyrosine kinase-like orphan receptor 1 (ROR1) is a member of the receptor tyrosine kinase family and consists of extracellular immunoglobulin-like domain, frizzled domain, kringle domain and

Abbreviations: NSCLC, non-small cell lung cancer; EGFR, epidermal growth factor receptor; ROR1, receptor tyrosine kinase-like orphan receptor 1; SPR, surface plasmon resonance; EGFR-TKIs, epidermal growth factor receptor-tyrosine kinase inhibitors; PI3K, phosphatidylinositol 3 kinase; AKT, protein kinase B; mTOR, mammalian target of rapamycin; HER3(ERBB3), human epidermal growth factor receptor 3; IGF-IR, insulin-like growth factor 1 receptor; CAR-T, chimeric antigen receptor T cells; CADD, computer-aided drug design; CETSA, cellular thermal shift assay; EdU, 5-ethynyl-2′-deoxyuridine; ADMET, absorption, distribution, metabolism, excretion and toxicity; TOPKAT, toxicity prediction by komputer assisted technology; IHC, immunohistochemical; RIP3, receptor-interacting serine/threonine-protein kinase 3

* Corresponding author. State Key Laboratory of Biotherapy and Cancer Center, National Clinical Research Center for Geriatrics, West China Hospital, Sichuan University, Chengdu 610041, China, Renmin South Road, Section 3-17, Chengdu 610041, China.
** Corresponding author. State Key Laboratory of Biotherapy and Cancer Center, National Clinical Research Center for Geriatrics, West China Hospital, Sichuan University, Chengdu 610041, China, Renmin South Road, Section 3-17, Chengdu 610041, China.
E-mail addresses: xiaweiwei@scu.edu.cn (X.-W. Wei), yongpeng@scu.edu.cn (Y. Peng).
[1] These authors contribute equally to this work.

https://doi.org/10.1016/j.canlet.2019.05.016
Received 29 January 2019; Received in revised form 14 May 2019; Accepted 15 May 2019

intracellular tyrosine kinase domain in structure [8]. Emerging evidence shows that ROR1 is aberrantly overexpressed in various malignancies including ovarian, colorectal, lung cancers and leukemia, playing an important role in cancer development [9–14]. For instance, ROR1 interacts with the protein TCL1 to accelerate chronic lymphocytic leukemia progression in Eμ-TCL1 transgenic mice [15]. The long noncoding RNA MAYA mediates the crosstalk between ROR1-HER3 and Hippo-YAP pathways to promote bone metastasis of breast cancer [16]. ROR1 is also crucial for lung cancer progression, where the oncogenic transcription factor NKX2-1 induces ROR1 expression to sustain EGFR survival signaling [17]. A recent study reveals that ROR1 functions as a scaffold of cavin-1 and caveolin-1 for preventing lysosomal degradation of caveolin-1, giving that ROR1 inhibition can overcome EGFR-TKIs resistance via bypass MET and IGF-IR signaling [18]. Therefore, ROR1 is a potential therapeutic target for NSCLC treatment, especially for overcoming EGFR-TKIs-induced drug resistance.

The therapeutic potential of ROR1 in human cancer has been elucidated by monoclonal antibody or chimeric antigen receptor T cells (CAR-T) based therapy. ROR1-specific monoclonal antibodies were demonstrated to be effective to suppress breast cancer and leukemia [19–22]. Currently, the antibody Cirmtuzumab has been submitted to the phase I clinical trial in patients with chronic lymphocytic leukemia [23]. Additionally, the immunotherapy by ROR1-specific CAR-T cells showed significant antitumor activity for ROR1-positive tumors [24–28]. However, to the best of our knowledge, nearly no small molecule targeting ROR1 has been reported. Although small molecule KAN0439834 was found to induce apoptosis of chronic lymphocytic leukemia and pancreatic carcinoma cells by targeting ROR1, the authors did not publish its chemical structure [29,30]. Thus, the investigation of small molecule ROR1 inhibitors is still in its infancy.

In this work, we took advantage of the computer-aided drug design (CADD) and cell-based activity screening, and discovered the small molecule ARI-1 as a potent ROR1 inhibitor targeting ROR1 extracellular frizzled domain. ARI-1 significantly suppressed NSCLC both *in vitro* and in xenograft mice, and specially overcame EGFR-TKIs resistance in a ROR1-dependent manner, providing an attractive drug candidate for NSCLC treatment.

2. Materials and methods

2.1. Homologous modeling, computer-aided virtual screening and flexible docking

The amino acid sequence of ROR1 frizzled domain was obtained from UniProt website (https://www.uniprot.org, Entry: Q01973). The calculated 3D structure of frizzled domain was simulated via homologous modeling on SWISS-MODEL website (www.swissmodel.expasy.org) based on the amino acid sequence. In Discovery Studio v3.1 software, we established molecular docking model, and performed virtual screening and flexible docking following GOLD docking and Flexible docking protocols, respectively. The images of molecular docking results were processed by PyMOL v1.8 software.

2.2. Preparation of recombinant protein

The sequence encoding the extracellular frizzled domain of ROR1 (amino acid residues of 61–393) was amplified by PCR using the forward primer (TCGCGGATCCATGCATCACCATCACCATCACGATGAACC AATGAATAACATC) and the reverse primer (CAGTCTCGAGTTATGAA TCGCACGCTGGGATGT), and then cloned into pFastBac™ HT^b vector (Invitrogen, USA) at *Bam*HI and *Xho*I sites. The resultant plasmid was confirmed by Sanger sequencing and transformed into *E. coli.* DH10Bac to generate recombinant bacmid DNA, which was then transfected into *Spodoptera frugiperda* (Sf9) insect cells to produce baculovirus. After 3-round amplification, the baculovirus infected High Five cells to express the N-terminal His-tagged frizzled domain of ROR1. The recombinant protein was purified with Ni-NTA affinity agarose resin (GE Healthcare, USA), eluted with elution buffer (20 mM Tris-HCl, 150 mM NaCl, 300 mM imidazole, pH8.0), and further purified with Q-ion-exchange chromatography (GE Healthcare, USA).

2.3. Surface plasmon resonance (SPR)

The interaction between small molecule and ROR1 frizzled domain was evaluated by surface plasmon resonance (SPR) using a BIAcore T100 instrument (GE Healthcare, USA) following previous procedures with minor modification [31]. In brief, purified His-tagged ROR1 frizzled domain was immobilized on a carboxyl methylated dextran sensor chip (Sensor Chip CM3). A flow channel blocked by ethanolamine was used as control surface. The specific interaction of samples with the immobilized ROR1 frizzled domain was assessed. In preliminary assay for ROR1 occupation, Wnt5a protein (Wnt5a directly binds to ROR1 frizzled domain) was used as the positive control of ROR1 occupation. All samples were analyzed at a flow rate of 30 μL/min with 10 mM HEPES running buffer and contact time of 130 s. The surface was washed and regenerated with a 10 mM glycine-HCl buffer at pH 3.0 for 30 s followed by a 30 min waiting time for dissolution after each experiment. The analyses were performed in BIAcore T100 evaluation software, version 2.0.2 (GE Healthcare, USA).

2.4. Patient samples

Primary NSCLC tumor tissues and their adjacent normal tissues were collected from West China Hospital (China), which was approved by the Ethics Committee of West China Hospital of Sichuan University. Written informed consent for research purposes was provided for the patients. The patients' tissues were dissected into small pieces, and grounded into powder in the liquid nitrogen. Subsequently, cell lysates were obtained by adding RIPA buffer into the powder, and sonicated to efficiently lyze the cells, followed by centrifugation at 12000 rpm for 15 min at 4 °C. The resultant supernatants were subjected to Immunoblotting analysis.

2.5. Cell culture and construction of stable cell lines

Human lung cancer cells (PC9, H1975, A549, H441 and H1299) were cultured at 37 °C in RPMI-1640 medium plus 10% fetal bovine serum (FBS) and antibiotics in a 5% CO_2 incubator. To prepare lentivirus, pLKO.1-derived or pLVX-puro derived lentiviral plasmids were co-transfected into 293TN cells with the packaging plasmid pCMV-dR8.2 dvpr and the envelope plasmid pCMV-VSVG. At 48 h after transfection, viruses were concentrated by the PEG-it Virus precipitation solution (System Biosciences) and used to infect human lung cancer cells. Pools of stable transfectants were selected by puromycin selection. The sequences of shRNAs targeting ROR1 are CCCAGTGAG TAATCTCAGT (shROR1-1) and CCCAGAAGCTGCGAACTGT (shROR1-2).

2.6. ROR1 expression by flow cytometric analysis

Cells were seeded in a 6-well plate and cultured for 48 h, then collected and washed 3 times with phosphate-buffered saline (PBS) containing 2% FBS. Approximately 1×10^6 cells were incubated for 30 min with APC-conjugated anti-human ROR1 (Biolegend, cat#357806) or control IgG (Biolegend, cat#400120). After washing, cells were resuspended and subject to flow cytometry on a FACSCalibur instrument (BD Biosciences). Data were analyzed by FlowJo 7.6.2 software.

2.7. MTT assay

Cells were seeded in a 96-well plate (1500/well) and cultured

overnight, then the compounds dissolved in DMSO at varied concentrations was added to the medium. After 72 h treatment, MTT solution was added and incubated at 37 °C for 4 h. DMSO was added to dissolve the MTT-formazan crystal and the OD_{570nm} values of each well were determined by Microplate Reader. The IC_{50} value was calculated from parallel experiments via Graphpad Prism 6.0 software.

2.8. Cellular thermal shift assay (CETSA)

The CETSA assay was performed under the guidance of previous work [32,33]. The lysates of H1299 cells stably expressing flag-tagged ROR1 were divided into smaller aliquots (35 μL) and incubated with ARI-1 (5 μM) or vehicle at different temperatures for 3 min in T100 Thermal Cycler (BioRad, USA) followed by cooling for 3 min on ice. The heated aliquots were then centrifuged at 20,000 × *g* for 20 min at 4 °C in order to separate the soluble fractions from precipitates. The supernatants are subjected to SDS-PAGE and immunoblotting against anti-flag antibody. The intensity of protein was quantified by ImageJ software and normalized to the value at 54 °C.

2.9. EdU assay

The EdU assay was conducted under the guidance of our previous work with some modification [34]. After treatment with ARI-1 (15 μM) for 96 h, cells were incubated with 50 μM of EdU labeling media for 2 h in a 5% CO_2 incubator at 37 °C, followed by fixation with 4% paraformaldehyde for 15 min at room temperature and treatment with 0.5% Triton X-100 for 10 min at room temperature. Then cells were stained with Apollo reaction solution, washed three times with cold PBS, and further stained with Hoechst 33342 for 30 min. After washing, the cells were analyzed under fluorescence microscope (Olympus, Japan) and Flow cytometer (BD Biosciences, America). The EdU incorporation rate was analyzed as the ratio of EdU-positive cells to total Hoechst 33342-positive cells.

2.10. Colony formation assay

Approximately 3000 NSCLC cells were seeded in 6-well plates and treated with ARI-1 (15 μM) in a 5% CO_2 incubator. After 7 days, cells were fixed with 4% polyoxymethylene and stained with crystal violet. The images for colony formation was recorded by high-resolution scanner.

2.11. Flow cytometric analysis for apoptosis

Briefly, cells treated with ARI-1 (15 μM) or vehicle for 72 h were harvested and washed with PBS, then resuspended in 200 μL of Annexin V binding buffer and stained with Annexin-V-fluorescein isothiocyanate (FITC) for 15 min on ice in the dark. Subsequently, cells were incubated with 5 μL of propidium iodide (PI) solution for 5 min, and subjected to flow cytometry on a FACSCalibur instrument (BD Biosciences). The cells in the FITC-positive fraction were regarded as apoptotic cells.

2.12. Immunoblotting

The cells were treated with ARI-1 (15 μM) for 72 h. Both adherent and floating cells were collected and lysed by RIPA buffer containing protease inhibitor and phosphase inhibitor cocktails. After protein concentration was detemined by BCA measurements, equivalent amounts of proteins were subjected to SDS-PAGE and electrically transferred onto PVDF membrane (Millipore, USA). Membrane was blocked for 1 h by 5% BSA at room temperature prior to incubation with antibodies against *p*-AKT, AKT, *p*-mTOR, mTOR, p-P38, cleaved-PARP, PCNA or actin at 4 °C overnight. After washed three times with TBST, membrane was incubated in horseradish peroxidase-conjugated second antibody for 1 h and washed three times with TBST. Finally the enhanced chemiluminescence detection (Amersham Biosciences, Sweden) kit was used to detect signals.

2.13. Wound-healing assay

NSCLC cells plated in 6-well plates overnight. When the cells reached 95% confluence, sterile pipette tips were used to scratch the wound uniformly. Cell motility in presence of the compound ARI-1 (15 μM) was assessed by measuring the migration of cells into a scraped wound. The wound-healing was monitored at 0 h, 24 h and 48 h by measuring the remaining area. The data were normalized the remaining area of corresponding groups at 0 h.

2.14. Transwell migration assay

NSCLC cells were seeded in the top chambers of 24-well invasion chambers with RPMI-1640 medium supplemented with 10% fetal bovine serum and 1% penicillin/streptomycin sulfate in the bottom chambers. Immediately, ARI-1 (15 μM) and vehicle were added to the top chambers. After 24 h, migration was terminated and the filters were fixed with 4% paraformaldehyde for 20 min and stained with crystal violet for 10 min. Graphic images were recorded using microscope. The data were normalized the corresponding migrated cells treated with vehicle.

2.15. Xenograft experiment

All animal experiments were performed according to the institutional ethical guidelines of animal care. BALB/c nude mice were subcutaneously implanted with 3×10^6 H1975 cells in 50% matrigel (injection volume of 100 μL/mouse). When the tumor volume reached about 150–200 mm^3, nude mice were randomly assigned into control and treatment groups (n = 5/group). The control group was given vehicle alone, and the treatment group received ARI-1 administration at the dosage of 5 mg/kg via intravenous injection every two day for 14 days. The tumor volume was calculated as follows: tumor volume = (length × $width^2$)/2.

2.16. Histopathology and immunohistochemistry

BALB/c nude mice bearing tumors were treated with ARI-1 (5 mg/kg) or vehicle as described above. After 14 days of dosing, individual mice were humanely euthanized, the samples of mice organs were collected and fixed with formalin and embedded in paraffin. Sections measuring 4–8 μm in thickness were prepared for hematoxylin and eosin (H&E) staining and immunostaining with antibody (anti-RIP3, Abcam). The liver of mice administrated with carbon tetrachloride was used as positive control in immunohistochemistry. The images were acquired on an Olympus digital camera attached to a light microscope.

2.17. Statistical analysis

All values are expressed as mean ± SD. Raw data were analyzed using Graphpad Prism 6.0 software. The statistical significance between experimental group and control was determined by Student's t-test or Wilcoxon's test. P values < 0.05 were considered statistically significant.

3. Results

3.1. ROR1 is a therapeutic target for NSCLC therapy

ROR1 is overexpressed in diverse types of human cancers and acts as an oncogene to promote cell proliferation and migration [35]. To confirm the therapeutic potential of ROR1, we analyzed ROR1 expression in NSCLC tumors and their adjacent normal tissues by

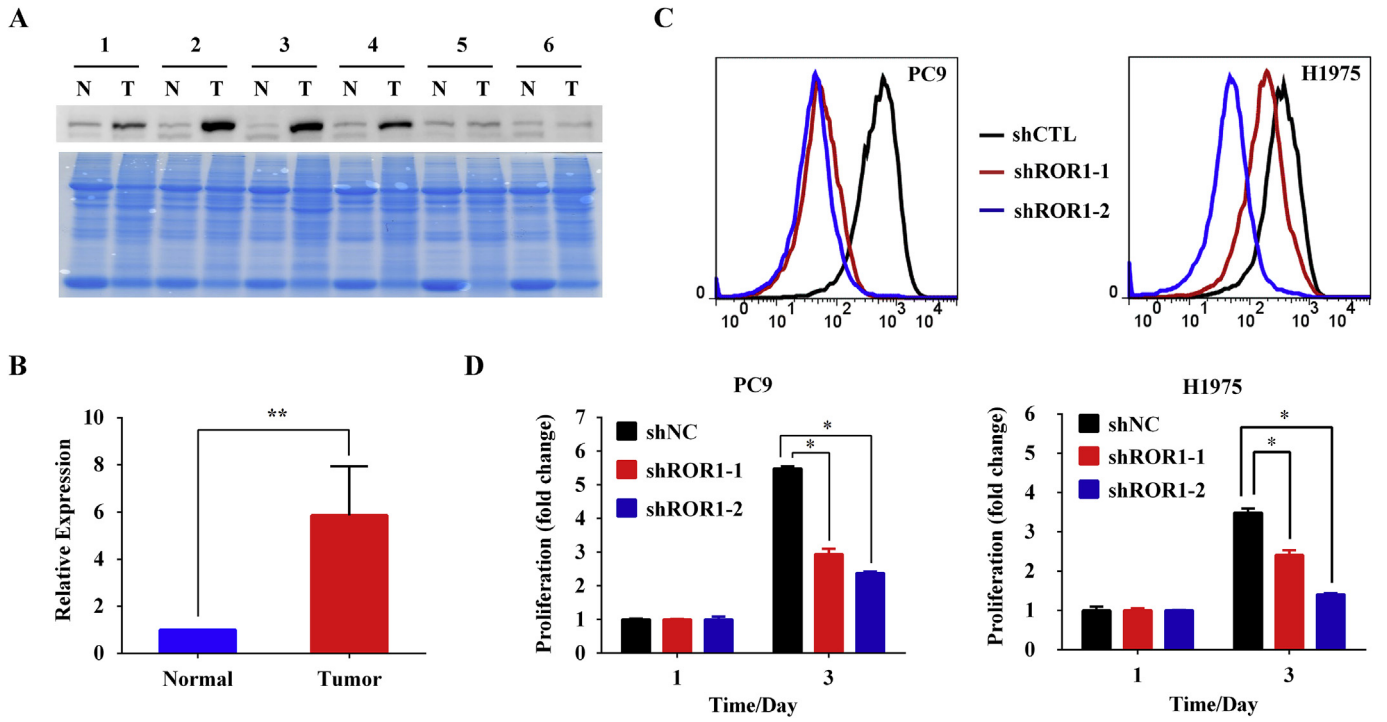

Fig. 1. ROR1 is a potential therapeutic target for NSCLC therapy. (A) Immunoblotting analysis and (B) quantification of ROR1 expression in NSCLC tumor tissues (T) and their adjacent normal tissues (N). Coomassie brilliant blue staining of the lysates of tumor and normal tissues was used as loading control. (C) Flow cytometric analysis of ROR1 expression in PC9 (left) and H1975 (right) cells transfected with ROR1-knockdown or control vectors. (D) Cell proliferation measured by MTT assays of PC9 (left) and H1975 (right) cells with or without ROR1 knockdown. (For interpretation of the references to color in this figure legend, the reader is referred to the Web version of this article.)

immunoblotting analysis. The results indicated that ROR1 was aberrantly overexpressed in NSCLC (Fig. 1A and B). Furthermore, we established the stable PC9 and H1975 cells with ROR1-knockdown by shRNAs (Fig. 1C). Consistent with previous results [36], ROR1 knockdown remarkably reduced cell proliferation in both PC9 and H1975 cells (Fig. 1D), suggesting that ROR1 is a promising target for NSCLC therapy.

3.2. Computer-aided screening and chemical synthesis of ROR1 inhibitors

ROR1 consists of the extracellular immunoglobulin-like domain, the frizzled domain, the kringle domain and the intracellular tyrosine kinase domain in structure [8]. Upon recognizing its ligand Wnt5a, the extracellular frizzled domain of ROR1 activates its downstream oncogenic signaling pathways, indicating that the frizzled domain is a key motif for ROR1 function (Fig. 2A) [37–40]. However, its 3D structure was not dissected until now. Our bioinformatics analysis shows that the amino acid sequence of ROR1 frizzled domain have high identity with that of MUSK (muscle, skeletal receptor tyrosine-protein kinase), therefore we simulated the 3D structure of ROR1 frizzled domain via homology modeling in SWISS-MODEL website using MUSK as template [41]. The simulative 3D structure composed of four α-helixes and a β-sheet (Fig. 2B). Small molecules in a library containing 15133 compounds were screened *in silico* through GOLD molecular docking. Higher GoldScore.Fitness value implies higher potential affinity between protein and small molecules. Top-30 ranking hits were then submitted to the cell-based activity assay to evaluate their inhibitory activity in NSCLC cells. The results suggested several hits had desirable activity (Fig. 2C). Intriguingly, a majority of bioactive hits shared a common "(*R*)-2-phenylchroman-4-one" skeleton, also known as (*R*)-flavanone (Fig. 2D). Thus, we speculated that (*R*)-flavanone derivatives were favorable to inhibit ROR1 function.

To verify this speculation, a series of (*R*)-flavanone derivatives synthesized by asymmetric 1,4-addition of phenylboronic acids to chromones catalyzed by Pd $(TFA)_2$/(*S*)-*t*BuPyOX system [42,43]. Starting from diverse substituted arylboronic acids and chromone, the enantiomeric compounds **1–20** were successfully prepared for the surface plasmon resonance (SPR) assay and the MTT assay at the sample concentrations of 5 μM and 50 μM, respectively (Fig. 2E and S1). Recombinant extracellular ROR1 proteins were expressed in baculovirus expression system and purified by affinity chromatography (Fig. 2F). Compound **3** exhibited both good affinity to ROR1 frizzled domain and potent inhibitory activity against H1975 cells (Fig. 2G, Table 1), providing a favorable lead structure for ROR1 inhibitor.

To obtain better bioactive molecules based on compound **3**, we next synthesized compounds **21–40** by Pd $(TFA)_2$/(*S*)-*t*BuPyOX-catalyzed asymmetric conjugate addition of 4′-methoxylphenylboronic acid to diverse chromones (Fig. 2E and S2). Compounds **41** and **42** were afforded by the deprotection from compound **39** and **40** (Fig. 2E and S2). The results of SPR assay and MTT assay suggested compound **39** ((*R*)-5,7-bis(methoxymethoxy)-2-(4-methoxyphenyl)chroman-4-one, thereafter referred as ARI-1) was the most potent and bioactive ROR1 inhibitor with 88.07% of ROR1 occupation at 5 μM and 93.44% of NSCLC inhibition at 50 μM (Fig. 2H and I, Table 2), giving a potential lead compound for NSCLC treatment.

3.3. ARI-1 directly interacts with the ROR1 frizzled domain

To further check the *in vitro* interaction between ROR1 and ARI-1, we performed cellular thermal shift assay (CETSA) and SPR assay to characterize the protein-small molecule interaction. The stable H1299 cells with Flag-ROR1 overexpression were established for CETSA experiments (Fig. 3A). As shown in Fig. 3B and C, ARI-1 significantly increased the thermal stability of ROR1 with a temperature shift of 1.715 °C, indicating the direct binding of ARI-1 with ROR1. Moreover, SPR assays further confirmed the strong binding affinity of ARI-1 with ROR1 *in vitro* with a dissociation constant (K_d value) of 0.468 μM (Fig. 3D). To interpret the structural basis of ROR1-ARI-1

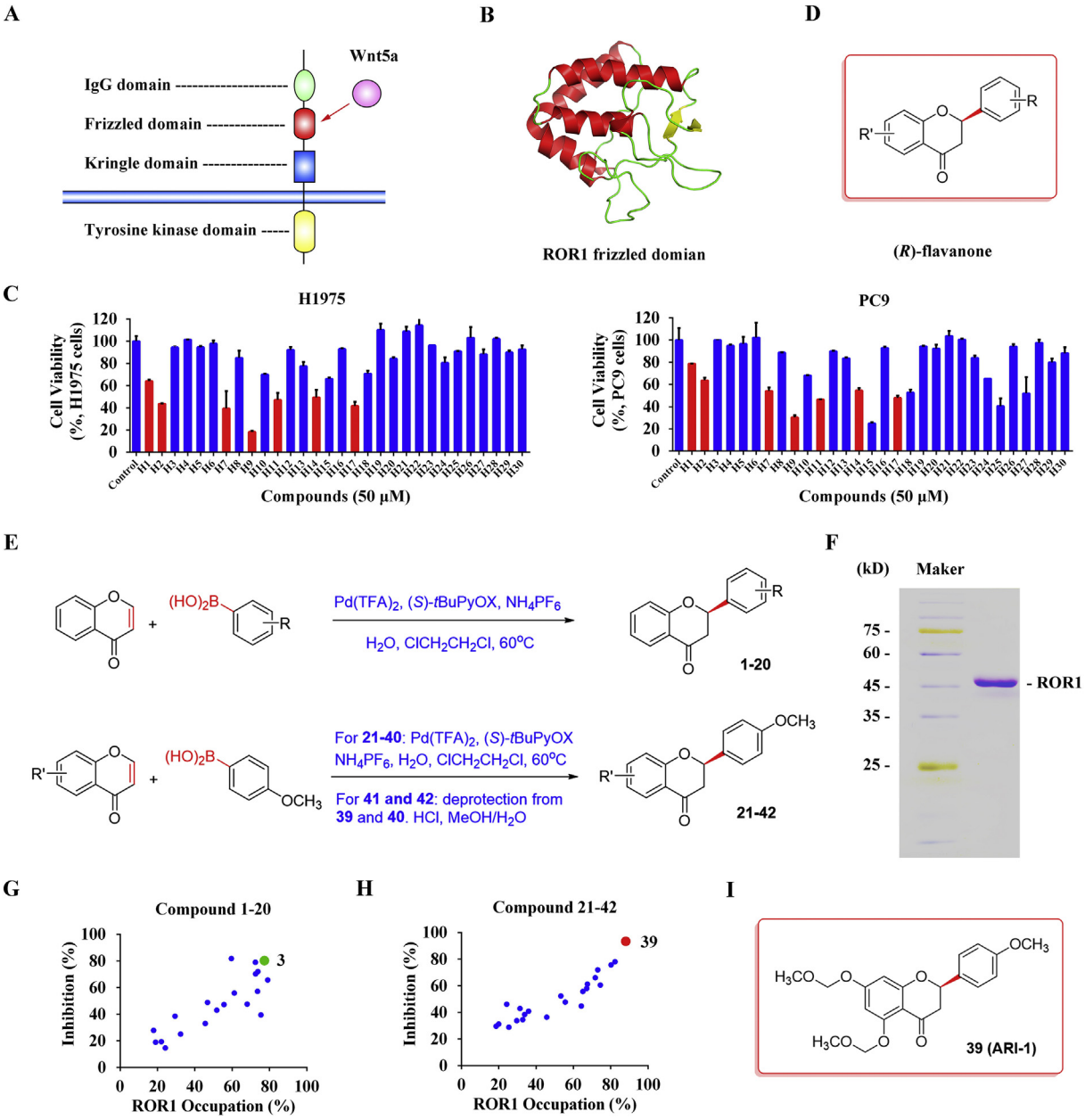

Fig. 2. Computer-aided drug screening and chemical synthesis of ROR1 inhibitors. (A) ROR1 consists of extracellular immunoglobulin-like domain, frizzled domain, kringle domain and intracellular tyrosine kinase domain. (B) 3D structure of ROR1 frizzled domain via homology modeling based on the amino acid sequence. (C) Cell proliferation of H1975 (left) and PC9 (right) cells treated with hit compounds (H1–H30) at the concentration of 50 μM. The red-colored compounds are (*R*)-flavanones. (D) Chemical structure of (*R*)-flavanones. (E) Synthesis of (R)-flavanones via asymmetric conjugate addition of substituted acids to chromones and deprotection. (F) Coomassie brilliant blue staining of purified extracellular ROR1 frizzled domain. (G, H) Biological screening of ROR1 inhibitors by SPR and MTT assays. Compound **3** (green in G) and compound **39** (red in H) are the optimal inhibitors, respectively. (I) Chemical structure of compound **39** (ARI-1). (For interpretation of the references to color in this figure legend, the reader is referred to the Web version of this article.)

interaction, we simulated the binding pattern of ROR1 and ARI-1 via the flexible docking in Discovery Studio software. The data showed that ARI-1 directly bound to the ROR1 frizzled domain through the amino acid residues of Lys314 and His427 by hydrogen bond and π-cation interaction, respectively (Fig. 3E). Furthermore, residue Leu429 was also pivotal, because it gave steric hindrance for the ROR1-ARI-1 binding. Therefore, these data provide the experimental and *in silico* evidences for the ROR1-ARI-1 interaction.

3.4. ARI-1 inhibits cell proliferation and induces apoptosis by blocking PI3K/AKT/mTOR pathway

With the ROR1 inhibitor ARI-1 in hand, we subsequently assessed its cellular function in NSCLC cells. In MTT assays, ARI-1 significantly suppressed cell proliferation in H1975, PC9 and H441 cells (with high ROR1 expression), but was insensitive to H1299 and A549 cells (with low ROR1 expression) (Fig. 4A and S3, Table S1), suggesting that ARI-1 specifically targets ROR1. Moreover, EdU assays and colony formation experiments indicated that ARI-1 treatment remarkably inhibited DNA replication and cell growth in both H1975 and PC9 cells (Fig. 4B and C and S4), giving additional evidence for the NSCLC inhibitory function

Table 1
Biological activity of compound 1-20.

Compound	SPR assay (5 μM) (% of occupation)	MTT assay (50 μM) (% inhibition)	Compound	SPR assay (5 μM) (% of occupation)	MTT assay (50 μM) (% inhibition)
1	68.04 ± 6.83	47.59 ± 4.92	**11**	22.08 ± 3.95	19.44 ± 5.49
2	73.79 ± 2.95	72.07 ± 3.48	**12**	55.64 ± 7.12	47.25 ± 3.06
3	77.32 ± 5.04	80.33 ± 7.46	**13**	45.60 ± 3.66	33.05 ± 5.41
4	51.77 ± 6.98	43.04 ± 6.07	**14**	19.02 ± 3.46	19.03 ± 3.55
5	72.49 ± 3.74	79.03 ± 4.26	**15**	17.95 ± 5.28	27.88 ± 6.01
6	61.18 ± 4.27	55.95 ± 7.04	**16**	24.22 ± 6.91	14.71 ± 5.38
7	32.38 ± 2.81	25.08 ± 2.08	**17**	46.85 ± 6.07	48.88 ± 4.48
8	72.56 ± 7.42	70.34 ± 6.86	**18**	75.45 ± 9.36	39.54 ± 6.11
9	29.39 ± 3.35	38.59 ± 5.31	**19**	79.05 ± 7.37	65.72 ± 3.19
10	59.57 ± 6.73	81.83 ± 8.87	**20**	73.61 ± 4.28	57.16 ± 7.21

Table 2
Biological activity of compound 21-42.

Compound	SPR assay (5 μM) (% of occupation)	MTT assay (50 μM) (% inhibition)	Compound	SPR assay (5 μM) (% of occupation)	MTT assay (50 μM) (% inhibition)
21	73.03 ± 6.45	72.03 ± 4.39	**32**	53.27 ± 2.12	52.41 ± 6.48
22	65.06 ± 6.89	55.72 ± 5.83	**33**	25.38 ± 4.23	28.89 ± 4.81
23	64.24 ± 3.23	44.85 ± 6.02	**34**	67.50 ± 6.35	61.30 ± 7.22
24	45.68 ± 9.89	36.47 ± 2.64	**35**	29.61 ± 8.46	33.79 ± 9.63
25	67.10 ± 2.31	58.08 ± 3.25	**36**	71.73 ± 4.58	66.11 ± 2.04
26	18.52 ± 2.73	29.70 ± 5.87	**37**	33.84 ± 2.69	38.52 ± 4.44
27	19.94 ± 4.15	31.32 ± 7.49	**38**	35.96 ± 4.81	40.92 ± 6.85
28	31.37 ± 5.57	42.95 ± 9.11	**39**	88.07 ± 6.92	93.44 ± 6.26
29	32.79 ± 6.99	34.55 ± 3.72	**40**	80.19 ± 9.04	75.74 ± 4.67
30	24.21 ± 8.41	46.17 ± 2.34	**41**	82.30 ± 6.15	78.15 ± 4.07
31	55.63 ± 9.83	47.79 ± 3.96	**42**	74.42 ± 8.27	60.55 ± 6.48

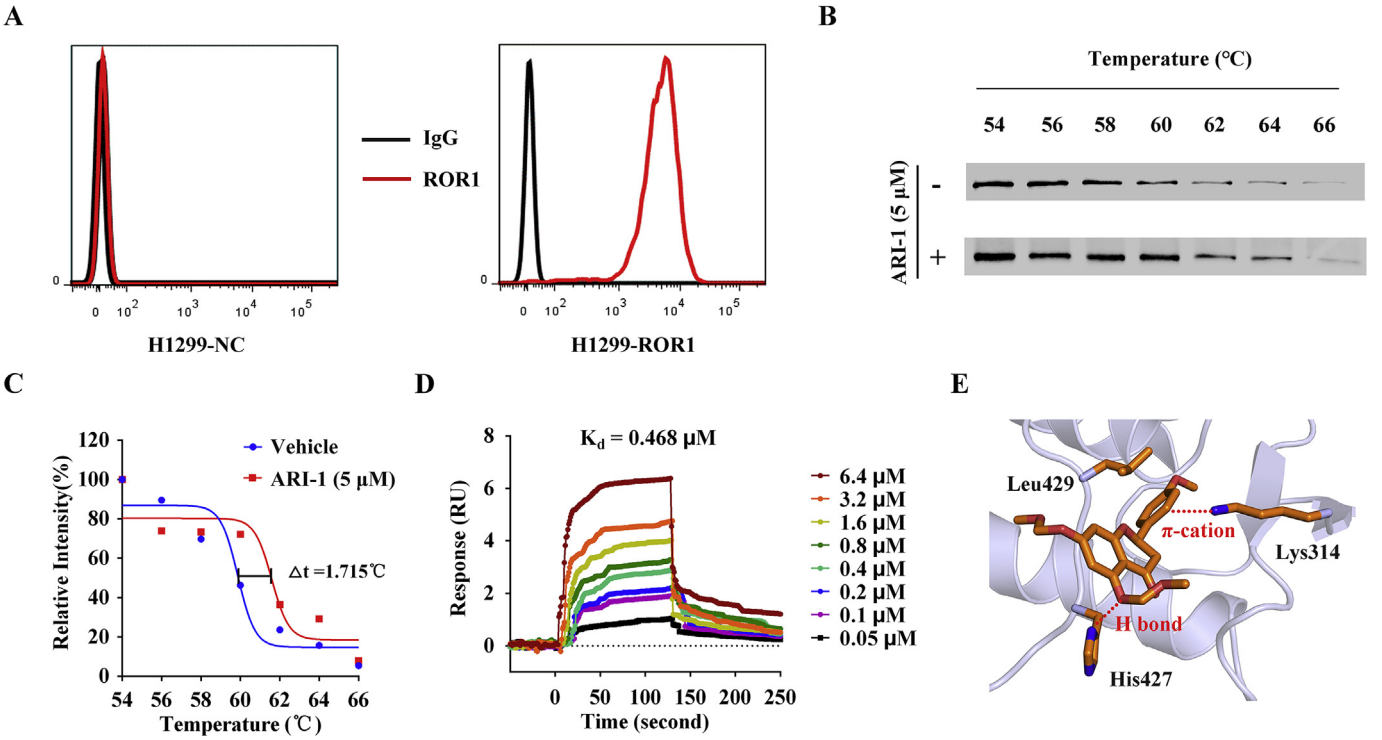

Fig. 3. ARI-1 directly binds to the frizzled domain of ROR1. (A) Flow cytometric analysis of H1299 cells stably transfected with flag-ROR1-overexpressing (H1299-ROR1) and control (H1299-NC) vectors. (B) Cellular thermal shift assays (CETSA) from 54 to 66 °C in the flag-ROR1-overexpressed H1299 cell lysates with or without ARI-1 (5 μM) incubation. The representative images were obtained by immunoblotting against anti-flag antibody. (C) Quantification of CETSA from 54 to 66 °C in flag-ROR1-overexpressed H1299 cell lysates with or without ARI-1 (5 μM) incubation. The data were normalized to the intensity of protein at 54 °C. (D) Surface plasmon resonance (SPR) assays of the immobilized extracellular ROR1 frizzled domain toward varied concentrations of ARI-1. (E) The representative image of flexible docking between ROR1 frizzled domain and ARI-1.

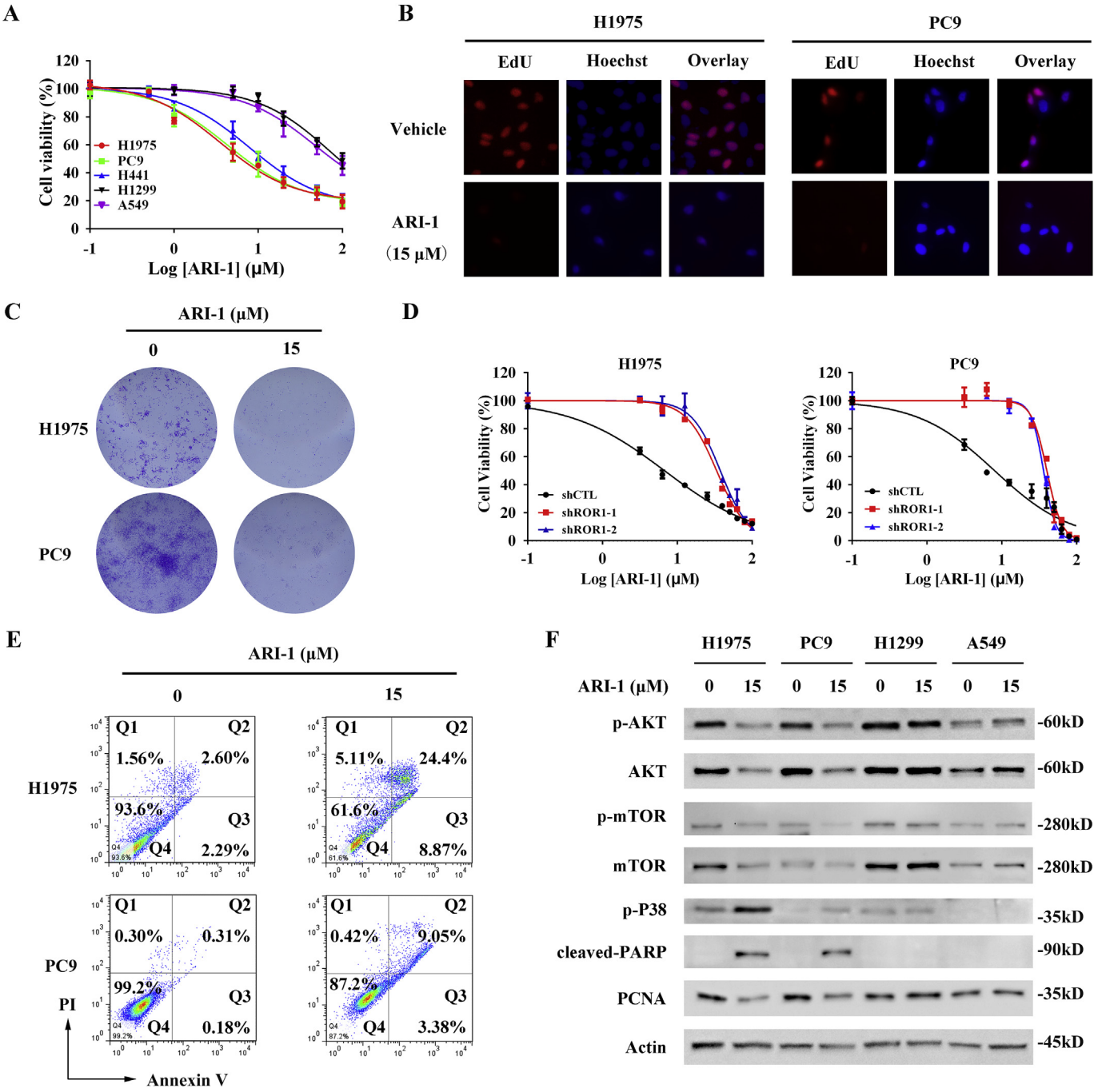

Fig. 4. ARI-1 inhibits cell proliferation and induces apoptosis by blocking PI3K/AKT/mTOR pathway. (A) MTT assays of lung cancer cells (H1975, PC9, H441, H1299 and A549) treated with or without varied concentrations of ARI-1. (B,C) Effect of ARI-1 (15 μM) treatment on cell growth in H1975 and PC9 cells, measured by EdU cell proliferation assay and colony formation assay. (D) Measurement of cell proliferation by MTT assay of ROR1-knockdown or control H1975 (left) or PC9 (right) cells treated with varied concentration of ARI-1. (E) Flow cytometric analysis of apoptotic cells after ARI-1 (15 μM) treatment in H1975 and PC9 cells. (F) Immunoblotting analysis on the levels of *p*-AKT, AKT, *p*-mTOR, mTOR, p-P38, cleaved-PARP, PCNA and actin in H1975, PC9, H1299 and A549 cells upon ARI-1 (15 μM) treatment.

of ARI-1. To check the specificity of ARI-1 to ROR1, the stable H1975 and PC9 cells with or without ROR1 knockdown were treated with different concentration of ARI-1, and the results showed that ROR1 knockdown dramatically attenuated the anti-proliferative activity of ARI-1 (Figs. 4D and 1C), further supporting ARI-I specificity toward ROR1. As H1975 cells were gefitinib-resistant NSCLC cells, ARI-1 could overcame gefitinib resistance when ROR1 was overexpressed, indicating a clue to overcome gefitinib resistance in NSCLC cells.

Blockade of ROR1 signaling was reported to inhibit proliferation and also induce apoptosis of cancer cells via PI3K/AKT/mTOR signaling pathway [36,44]. Thus, to investigate the mechanism of ARI-1, we performed flow cytometry and immunoblotting. The flow cytometry experiments using annexin V-FITC/PI staining showed that NSCLC cells treated with ARI-1 had an increased proportion of apoptosis cells (from 4.89% to 33.27% in H1975 cells, from 0.49% to 12.43% in PC9 cells) (Fig. 4E), indicating that ARI-1 significantly induced apoptosis in NSCLC cells. But its apoptosis-inducing function was inactive in H1299 and A549 cells (with low ROR1 level) (Figure S5). Immunoblotting analysis revealed that ARI-1 decreased the level of phosphorylated-AKT, AKT, phosphorylated-mTOR, mTOR and PCNA (proliferation

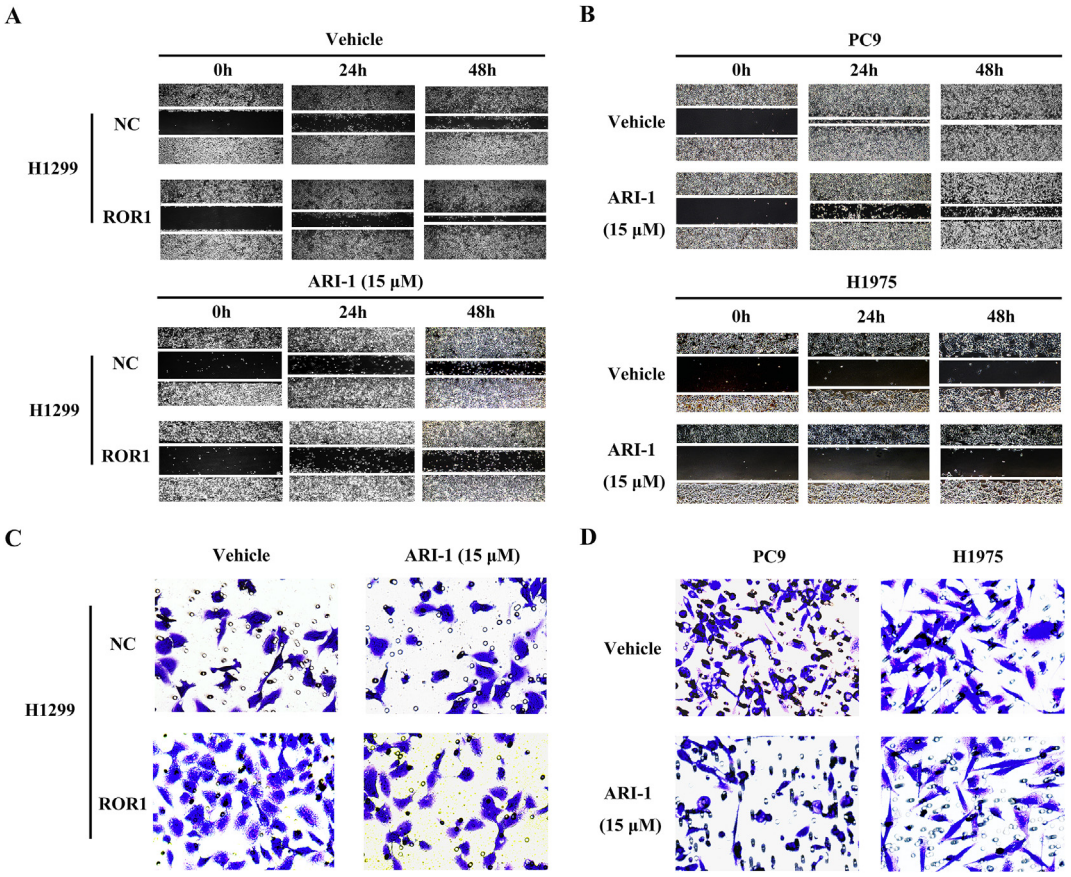

Fig. 5. ARI-1 suppresses cell migration in a ROR1-dependent manner in NSCLC cells. (A) The representative images of wound-healing assay in ROR1-overexpressing or negative control H1299 cells with or without ARI-1 (15 μM) incubation. (B) The representative images of H1975 and PC9 cells treated with or without ARI-1 (15 μM) in wound-healing assay. (C) The representative images of Transwell migration assay in ROR1-overexpressing or negative control H1299 cells with or without ARI-1 (15 μM) incubation. (D) The representative images of H1975 and PC9 cells treated with or without ARI-1 (15 μM) in Transwell migration assay.

marker), and increased the level of cleaved-PARP and p-P38 (apoptosis markers) in H1975 and PC9 cells (Fig. 4F and S6), suggesting that ARI-1 may suppress NSCLC by preventing the PI3K/AKT/mTOR signaling. However, ARI-1 nearly had no effect on PI3K/AKT/mTOR signaling in H1299 and A549 cells (Fig. 4F and S6), indicating the ROR1-dependence of ARI-1 in NSCLC cells. Therefore, these results demonstrated that ARI-1 inhibits cell growth and induces apoptosis in NSCLC cells by blocking PI3K/AKT/mTOR signaling pathway.

3.5. ARI-1 suppresses cell migration in a ROR1-dependent manner in NSCLC cells

When H1299 cells stably transfected with ROR1-overexpressing (H1299-ROR1) and control (H1299-NC) vectors (Fig. 3A), we found that ROR1 obviously promoted cell migration in wound-healing assay (Fig. 5A and S7). ROR1 inhibition by ARI-1 reduced the migratory ability of H1299-ROR1 cells, but H1299-NC cells were nearly unchanged upon ARI-1 incubation (Fig. 5A and S7), suggesting that the inhibitory activity of ARI-1 depended on ROR1 level in NSCLC cells. Moreover, ARI-1 suppressed cell migration in native PC9 and H1975 cells with high ROR1 expression (Fig. 5B and S8). In accordance with the results of wound-healing assays, Transwell migration assays also indicated NSCLC cell migration was obviously inhibited by ARI-1 when ROR1 was highly expressed (Fig. 5C and D and S9). These data indicated that ARI-1 can suppress NSCLC cell migration in a ROR1-dependent manner.

3.6. ARI-1 suppresses tumor growth in xenograft mice

To evaluate the antitumor function of ARI-1 *in vivo*, we firstly performed *in silico* ADMET Descriptors and Toxicity Prediction (TOPKAT) calculations. The results indicated that ARI-1 showed no or low toxicity in most toxicity prediction models (Table S2), exhibiting acceptable druggability. In xenograft model of nude mice, ARI-1 significantly inhibited H1975 tumor growth at the dosage of 5 mg/kg (Fig. 6A, B and 6C). Because ARI-1 has little effect on the body weights of BALB/c nude mice (Fig. 6D), so the tumor weight/body weight ratios were also suppressed upon ARI-1 administration (Fig. 6E). To examine the *in vivo* toxicity of ARI-1, we collected the liver tissues of nude mice injected with ARI-1 or vehicle, and performed immunohistochemical (IHC) analysis against RIP3 antibody (RIP3 is a biomarker of tissue necrosis). The positive control of liver necrosis was induced by the administration of carbon tetrachloride. As shown in Fig. 6F, ARI-1 did not cause obvious liver necrosis in nude mice. Moreover, the histopathology test revealed that ARI-1 had no remarkable toxicity to heart, liver, spleen, lung and kidney of nude mice (Fig. 6G). Together, these results demonstrate that ARI-1 had an attractive antitumor activity in xenograft model, providing a potential small moleuclar inhibitor for NSCLC treatment.

4. Discussion

NSCLC is the leading cause of cancer-related human death worldwide [2]. Currently, ROR1-targeted therapies based on monoclonal antibodies [19–23] and CAR-T cells [25–29] display remarkable antitumor activity against leukemia or solid tumors, demonstrating the

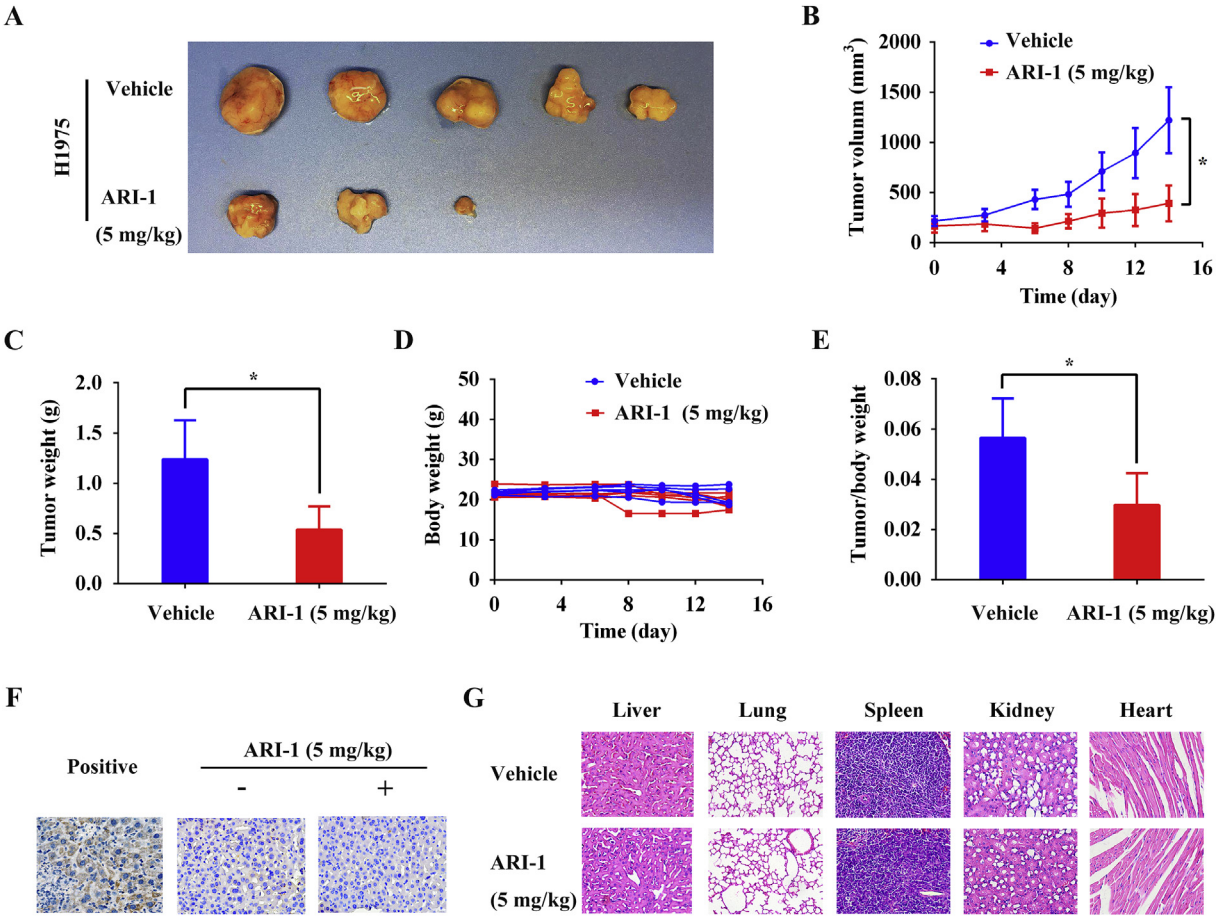

Fig. 6. ARI-1 suppresses NSCLC tumor growth without obvious toxicity. (A) The images of Balb/c nude mice tumor with or without the administration of ARI-1 for 14 days at the dosage of 5 mg/kg every two days. (n = 5 per group). (B) The nude mice tumor volumes measured for 14 days and (C) tumor weights of NSCLC xenograft tumors with or without ARI-1 administration (5 mg/kg). (D) Body weights of nude mice during the treatment of vehicle and ARI-1 (5 mg/kg) for 14 days. (E) Tumor weight/body weight ratios of xenograft nude mice upon vehicle and ARI-1 (5 mg/kg) for 14 days. (F) The representative images of immunohistochemistry analysis of liver from nude mice with or without ARI-1 (5 mg/kg) treatment for 14 days. The liver of mice administrated with carbon tetrachloride was used as positive control. (G) Histopathology test of liver, lung, spleen, kidney, and heart of nude mice with or without ARI-1 (5 mg/kg) injection for 14 days.

therapeutic role of ROR1 in human cancer, especially the potential to overcome EGFR-TKIs-induced drug resistance [18]. However, to the best of our knowledge, except for KAN0439834 (the author did not publish its structure) [29,30], no small molecule is reported as ROR1 inhibitors until now. Our work discovers ARI-1 as a novel small molecule-type ROR1 inhibitor. Experimental data indicate that ARI-1 potently inhibits NSCLC cells both *in vitro* and in xenograft model following a ROR1-dependent manner (Figs. 4–6). Importantly, ARI-1 is sensitive to NSCLC cells with high ROR1 level (Fig. 4A, D and 5), even though the cells are resistant to gefitinib, suggesting a drug candidate for the therapy of NSCLC with EGFR-TKIs resistance.

Structurally, ROR1 contains the immunoglobulin-like domain, the frizzled domain, the kringle domain and the tyrosine kinase domain [45]. Among them, the frizzled domain associates with Wnt5a to facilitate oncogenic signaling transduction and is crucial for cancer progression [37,46]. However, there is no report about the therapy targeting the frizzled domain. We took advantage of the computer-aided drug modeling and cell-based activity screening to find that (*R*)-flavanones are preferable to locate into frizzled domain with high potential affinity and the structural-matching hits as ROR1 inhibitors (Fig. 2C and D). The results of SPR assay and CETSA assay reveal the direct binding of ARI-1 to the frizzled domain of ROR1 (Fig. 3B and D). And this interaction is mediated by the amino acid residues Lys314, His427 and Leu429 of ROR1 (Fig. 3E). Considering the wide natural occurrence and effective synthetic methodology, (*R*)-flavanone is an ideal lead structure for compound optimization and drug development in future.

Increasing endeavor has been devoted to analyze the molecular behavior of ROR1 in cancer. Upon Wnt5a association, ROR1 activates NF-κB signaling and enhances the survival of chronic lymphocytic leukemia cells [47]. Moreover, ROR1 appears to participate in sustainment of EGF-induced signaling through the EGFR-ERBB3-PI3K axis, which is further upheld by ROR1 downstream through its kinase dependent c-Src activation [17]. Recent studies suggest several pathways including ERK, Hippo-YAP signaling pathways are also regulated by ROR1 [16]. Nevertheless, the molecular mechanism of ROR1 in promoting tumorigenesis and cancer progression remains obscure. So, the discovery of ARI-1 also provides a valuable molecular tool to probe the downstream signaling of ROR1, facilitating the clarification of the ROR1 mechanism in cancer.

In summary, we discovered ARI-1 as a novel ROR1 inhibitor directly targeting the frizzled domain with high binding affinity. Moreover, ARI-1 can potently inhibit NSCLC cell proliferation and migration through blocking PI3K/AKT/mTOR signaling pathway in a ROR1-dependent manner. Importantly, ARI-1 exhibits significant antitumor effect without obvious toxicity *in vivo*. Intriguingly, ARI-1 is effective to EGFR-TKIs-resistant NSCLC cells with high ROR1 expression. Hence, our study provides an attractive drug candidate for NSCLC treatment, especially for highly ROR1-expressed/EGFR-TKI-resistant NSCLC.

Funding

This work was supported by National Key R&D Program of China (No.2016YFA0502204 and 2017YFA0504304 to YP), National Natural Science Foundation of China (No.81772960 and 81572739 to YP; No.81702980 to WP), China Postdoctoral Science Foundation (No.2018M640925 to WP), Post-Doctor Research Project, West China Hospital, Sichuan University (No.2018HXBH014 to WP), the Sichuan Science and Technology Program (No. 2019JDTD0013) and the 1.3.5 Project for Disciplines of Excellence (No. ZYJC18030), West China Hospital, Sichuan University.

Competing interests

The authors declare no competing financial interests.

Appendix A. Supplementary data

Supplementary data to this article can be found online at https://doi.org/10.1016/j.canlet.2019.05.016.

References

[1] R.L. Siegel, K.D. Miller, A. Jemal, Cancer statistics, 2018, CA Cancer J. Clin. 67 (2018) 7–30.
[2] R.S. Herbst, D. Morgensztern, C. Boshoff, The biology and management of non-small cell lung cancer, Nature 553 (2018) 446–454.
[3] M. Reck, K.F. Rabe, Precision diagnosis and treatment for advanced non-small-cell lung cancer, N. Engl. J. Med. 377 (2017) 849–861.
[4] Z. Chen, C.M. Fillmore, P.S. Hammerman, C.F. Kim, K.K. Wong, Non-small-cell lung cancers: a heterogeneous set of diseases, Nat. Rev. Canc. 14 (2014) 535–546.
[5] S. Niessen, M.M. Dix, S. Barbas, Z.E. Potter, S. Lu, O. Broadsky, et al., Proteome-wide map of targets of T790M-EGFR-directed covalent inhibitors, Cell Chem Biol. 24 (2017) 1388–1400.e7.
[6] J.F. Gainor, A.T. Shaw, Emerging paradigms in the development of resistance to tyrosine kinase inhibitors in lung cancer, J. Clin. Oncol. 31 (2013) 3987–3996.
[7] K.S. Thress, C.P. Paweletz, E. Felip, B.C. Cho, D. Stetson, B. Dougherty, et al., Acquired EGFR C797S mutation mediates resistance to AZD9291 in non-small cell lung cancer harboring EGFR T790M, Nat. Med. 21 (2015) 560–562.
[8] G. Rebagay, S. Yan, C. Liu, N.K. Cheung, ROR1 and ROR2 in human malignancies: potentials for targeted therapy, Front Oncol. 2 (2012) 34.
[9] M.P. O'Connell, K. Marchbank, M.R. Webster, A.A. Valiga, A. Kaur, A. Vultur, et al., Hypoxia induces phenotypic plasticity and therapy resistance in melanoma via the tyrosine kinase receptors ROR1 and ROR2, Cancer Discov. 3 (2013) 1378–1393.
[10] B. Cui, E.M. Ghia, L. Chen, L.Z. Rassenti, C. DeBoever, G.F. 2nd Widhopf, et al., High-level ROR1 associates with accelerated disease progression in chronic lymphocytic leukemia, Blood 128 (2016) 2931–2940.
[11] A. Balakrishnan, T. Goodpaster, J. Randolph-Habecker, B.G. Hoffstrom, F.G. Jalikis, L.K. Koch, et al., Analysis of ROR1 protein expression in human cancer and normal tissues, Clin. Cancer Res. 23 (2017) 3061–3071.
[12] Y.Z. Zheng, R. Ma, J.K. Zhou, C.L. Guo, Y.S. Wang, Z.G. Li, et al., ROR1 is a novel prognostic biomarker in patients with lung adenocarcinoma, Sci. Rep. 6 (2016) 36447.
[13] J.K. Zhou, Y.Z. Zheng, X.S. Liu, Q. Gou, R. Ma, C.L. Guo, et al., ROR1 expression as a biomarker for predicting prognosis in patients with colorectal cancer, Oncotarget 8 (2017) 32864–32872.
[14] A. Gentile, L. Lazzari, S. Benvenuti, L. Trusolino, P.M. Comoglio, tumorigenesis, Cancer Res. 71 (2011) 3132–3141.
[15] G.F. 2nd Widhopf, B. Cui, E.M. Ghia, L. Chen, K. Messer, Z. Shen, et al., ROR1 can interact with TCL1 and enhance leukemogenesis in Eμ-TCL1 transgenic mice, Proc. Natl. Acad. Sci. U.S.A. 111 (2014) 793–798.
[16] C. Li, S. Wang, Z. Xing, A. Lin, K. Liang, J. Song, et al., A ROR1-HER3-lncRNA signalling axis modulates the Hippo-YAP pathway to regulate bone metastasis, Nat. Cell Biol. 19 (2017) 106–119.
[17] T. Yamaguchi, K. Yanagisawa, R. Sugiyama, Y. Hosono, Y. Shimada, C. Arima, et al., NKX2-1/TITF1/TTF-1-Induced ROR1 is required to sustain EGFR survival signaling in lung adenocarcinoma, Cancer Cell 21 (2012) 348–361.
[18] T. Yamaguchi, C. Lu, L. Ida, K. Yanagisawa, J. Usukura, J. Cheng, et al., ROR1 sustains caveolae and survival signalling as a scaffold of cavin-1 and caveolin-1, Nat. Commun. 7 (2016) 10060.
[19] A.H. Daneshmanesh, M. Hojjat-Farsangi, A.S. Khan, M. Jeddi-Tehrani, M.M. Akhondi, A.A. Bayat, et al., Monoclonal antibodies against ROR1 induce apoptosis of chronic lymphocytic leukemia (CLL) cells, Leukemia 26 (2012) 1348–1355.
[20] B. Cui, S. Zhang, L. Chen, J. Yu, G.F. 2nd Widhopf, J.F. Fecteau, et al., Targeting ROR1 inhibits epithelial-mesenchymal transition and metastasis, Cancer Res. 73 (2013) 3649–3660.
[21] J.T. Patterson, S. Asano, X. Li, C. Rader, C.F. 3rd Barbas, Improving the serum stability of site-specific antibody conjugates with sulfone linkers, Bioconjug. Chem. 25 (2014) 1402–1407.
[22] J. Yu, L. Chen, B. Cui, C. Wu, M.Y. Choi, Y. Chen, et al., Cirmtuzumab inhibits Wnt5a-induced Rac1 activation in chronic lymphocytic leukemia treated with ibrutinib, Leukemia 31 (2017) 1333–1339.
[23] M.Y. Choi, G.F. 2nd Widhopf, E.M. Ghia, R.L. Kidwell, M.K. Hasan, J. Yu, et al., Phase I Trial: Cirmtuzumab inhibits ROR1 signaling and stemness signatures in patients with chronic lymphocytic leukemia, Cell Stem Cell 22 (2018) 951–959 e3.
[24] M. Hudecek, T.M. Schmitt, S. Baskar, M.T. Lupo-Stanghellini, T. Nishida, T.N. Yamamoto, et al., The B-cell tumor-associated antigen ROR1 can be targeted with T cells modified to express a ROR1-specific chimeric antigen receptor, Blood 116 (2010) 4532–4541.
[25] M. Hudecek, M.T. Lupo-Stanghellini, P.L. Kosasih, D. Sommermeyer, M.C. Jensen, C. Rader, et al., Receptor affinity and extracellular domain modifications affect tumor recognition by ROR1-specific chimeric antigen receptor T cells, Clin. Cancer Res. 19 (2013) 3153–3164.
[26] C. Berger, D. Sommermeyer, M. Hudecek, M. Berger, A. Balakrishnan, P.J. Paszkiewicz, et al., Safety of targeting ROR1 in primates with chimeric antigen receptor-modified T cells, Cancer Immunol Res. 3 (2015) 206–216.
[27] M. Hudecek, D. Sommermeyer, P.L. Kosasih, A. Silva-Benedict, L. Liu, C. Rader, et al., The nonsignaling extracellular spacer domain of chimeric antigen receptors is decisive for in vivo antitumor activity, Cancer Immunol Res. 3 (2015) 125–135.
[28] J. Qi, X. Li, H. Peng, E.M. Cook, E.L. Dadashian, A. Wiestner, et al., Potent and selective antitumor activity of a T cell-engaging bispecific antibody targeting a membrane-proximal epitope of ROR1, Proc. Natl. Acad. Sci. U.S.A. 115 (2018) e5467–e5476.
[29] M. Hojjat-Farsangi, A.H. Daneshmanesh, A.S. Khan, J. Shetye, F. Mozaffari, P. Kharaziha, et al., First-in-class oral small molecule inhibitor of the tyrosine kinase ROR1 (KAN0439834) induced significant apoptosis of chronic lymphocytic leukemia cells, Leukemia 32 (2018) 2291–2295.
[30] A.H. Daneshmanesh, M. Hojjat-Farsangi, A. Ghaderi, A. Moshfegh, L. Hansson, J. Schultz, et al., A receptor tyrosine kinase ROR1 inhibitor (KAN0439834) induced significant apoptosis of pancreatic cells which was enhanced by erlotinib and ibrutinib, PLoS One 13 (2018) e0198038.
[31] D. Sun, J.K. Zhou, L. Zhao, Z.Y. Zheng, J. Li, W. Pu, et al., Novel curcumin liposome modified with hyaluronan targeting CD44 plays an anti-leukemic role in acute myeloid leukemia in vitro and in vivo, ACS Appl. Mater. Interfaces 9 (2017) 16857–16868.
[32] D. Martinez Molina, R. Jafari, M. Ignatushchenko, T. Seki, E.A. Larsson, C. Dan, et al., Monitoring drug target engagement in cells and tissues using the cellular thermal shift assay, Science 341 (2013) 84–87.
[33] W. Pu, J. Li, Y. Zheng, X. Shen, X. Fan, J.K. Zhou, et al., Targeting Pin1 by inhibitor API-1 regulates microRNA biogenesis and suppresses hepatocellular carcinoma development, Hepatology 68 (2018) 547–560.
[34] Q. Gou, L. Gao, X. Nie, W. Pu, J. Zhu, Y. Wang, et al., Long noncoding RNA AB074169 inhibits cell proliferation via modulation of KHSRP-mediated CDKN1a expression in papillary thyroid carcinoma, Cancer Res. 78 (2018) 4163–4174.
[35] N. Borcherding, D. Kusner, G.H. Liu, W. Zhang, ROR1, an embryonic protein with an emerging role in cancer biology, Protein Cell 5 (2014) 496–502.
[36] Y. Liu, H. Yang, T. Chen, Y. Luo, Z. Xu, Y. Li, et al., Silencing of receptor tyrosine kinase ROR1 inhibits tumor-cell proliferation via PI3K/AKT/mTOR signaling pathway in lung adenocarcinoma, PLoS One 10 (2015) e0127092.
[37] A. Sato, H. Yamamoto, H. Sakane, H. Koyama, A. Kikuchi, Wnt5a regulates distinct signaling pathways by binding to Frizzled2, EMBO J. 29 (2010) 41–54.
[38] M.K. Hasan, J. Yu, L. Chen, B. Cui, G.F. Widhopf Ii, L. Rassenti, et al., Wnt5a induces ROR1 to complex with HS1 to enhance migration of chronic lymphocytic leukemia cells, Leukemia 31 (2017) 2615–2622.
[39] J. Yu, L. Chen, Y. Chen, M.K. Hasan, E.M. Ghia, L. Zhang, et al., Wnt5a induces ROR1 to associate with 14-3-3ζ for enhanced chemotaxis and proliferation of chronic lymphocytic leukemia cells, Leukemia 31 (2017) 2608–2614.
[40] M.K. Hasan, J. Yu, G.F. Widhopf, L.Z. Rassenti, L. Chen, Z. Shen, et al., Wnt5a induces ROR1 to recruit DOCK2 to activate Rac1/2 in chronic lymphocytic leukemia, Blood 132 (2018) 170–178.
[41] Homology modeling of ROR1 frizzled domain on SWISS-MODEL, (2018) website at https://www.swissmodel.expasy.org/.
[42] X. Wang, B. Liu, X. Searle, C. Yeung, A. Bogdan, S. Greszler, et al., Discovery of 4-[(2R,4R)-4-({[1-(2,2-difluoro-1,3-benzodioxol-5-yl)cyclopropyl]carbonyl} amino)-7-(difluoromethoxy)-3,4-dihydro-2H-chromen-2-yl]benzoic acid (ABBV/GLPG-2222), a potent cystic fibrosis transmembrane conductance regulator (CFTR) corrector for the treatment of cystic fibrosis, J. Med. Chem. 61 (2018) 1436–1449.
[43] J.C. Holder, A.N. Marziale, M. Gatti, B. Mao, B.M. Stoltz, Palladium-catalyzed asymmetric conjugate addition of arylboronic acids to heterocyclic acceptors, Chem. Eur J. 19 (2013) 74–77.
[44] A.H. Daneshmanesh, M. Hojjat-Farsangi, A. Moshfegh, A.S. Khan, E. Mikaelsson, A. Österborg, et al., The PI3K/AKT/mTOR pathway is involved in direct apoptosis of CLL cells induced by ROR1 monoclonal antibodies, Br. J. Haematol. 169 (2015) 455–458.
[45] M. Hojjat-Farsangi, A. Moshfegh, A.H. Daneshmanesh, A.S. Khan, E. Mikaelsson, A. Osterborg, et al., The receptor tyrosine kinase ROR1–an oncofetal antigen for targeted cancer therapy, Semin. Canc. Biol. 29 (2014) 21–31.
[46] J. Cao, X. Wang, T. Dai, Y. Wu, M. Zhang, R. Cao, et al., Twist promotes tumor metastasis in basal-like breast cancer by transcriptionally upregulating ROR1, Theranostics 8 (2018) 2739–2751.
[47] T. Fukuda, L. Chen, T. Endo, L. Tang, D. Lu, J.E. Castro, et al., Antisera induced by infusions of autologous Ad-CD154-leukemia B cells identify ROR1 as an oncofetal antigen and receptor for Wnt5a, Proc. Natl. Acad. Sci. U.S.A. 105 (2008) 3047–3052.